

L. M. 9-L.

JUL 26 1939

5341
Guidonia

~~_____~~

TECHNICAL MEMORANDUMS
NATIONAL ADVISORY COMMITTEE FOR AERONAUTICS

No. 901

INVESTIGATIONS AND EXPERIMENTS
IN THE GUIDONIA SUPERSONIC WIND TUNNEL

By Antonio Ferri

Hauptversammlung der Lillenthal-Gesellschaft für
Luftfahrtforschung, Berlin, October 12-15, 1938

FILE COPY

*To be returned to
the files of the Langley
Memorial Aeronautical
Laboratory.*

Washington
July 1939

1.1.2.2
1.1.2.1
1.2.1
9.2

3 1176 00506 7070

NATIONAL ADVISORY COMMITTEE FOR AERONAUTICS

TECHNICAL MEMORANDUM NO. 901

INVESTIGATIONS AND EXPERIMENTS
IN THE GUIDONIA SUPERSONIC WIND TUNNEL*

By Antonio Ferri

INTRODUCTION

The initial period of activity at the supersonic wind tunnel at Guidonia was devoted to the problem of designing and building the experimental equipment necessary for systematic research. This equipment consisted primarily of

- 1) A number of different subsonic and supersonic cones or ducts designed to generate the desired speed in the experiment chamber.
- 2) An aerodynamic balance.
- 3) Optical instruments operating on the Schlieren and interferometric principle.

This period of study was long and laborious since practically no previous experimental data were available for guidance. Progress was of necessity slow before any definite decision could be made. During this period we designed a number of speed cones, an aerodynamic balance, and an optical plant, which, although in part still under construction, may be looked upon as being the final products.

It might be of interest to point out the points of view which emerged from completed experiments with the aid of such provisory equipment. Parallel with this activity some systematic studies in the field of sound were carried out, resulting in part in altogether new results.

*"Untersuchungen und Versuche im Überschallwindkanal zu Guidonia," Reprint of paper presented at meeting of Lillienthal-Gesellschaft für Luftfahrtforschung, October 12-15, 1938, Berlin.

PART I

EXPERIMENTAL EQUIPMENT

Subsonic and Supersonic Cones

The first task was the construction of the speed cones. They may be considered as consisting of two separate parts: the Laval nozzle or "effuser" for creating the velocity and the so-called diffuser, the inversely operating Laval nozzle. While there are rigorous criteria of design for the "effuser," they are almost completely lacking for the study of the diffuser, although it forms the most sensitive part of the cone.

After having found many guiding principles under its erstwhile director, Doctor Gasperi, for correct diffuser design, the efforts are now concentrated again on the study of a satisfactory effuser. Then the other problem is to be attacked again. For these investigations the choice fell to effusers with fixed walls; the problem of designing an effuser with adjustable walls was dropped for the time being although it had been studied at the very beginning, since it was impossible to predict the accuracy with which the adjustable channel could be approximated to a theoretical profile limitation, i.e., what degree of adjustability was necessary, and such a complicated construction could not be started because of the great probability of failure. For the diffuser, on the other hand, adjustable walls should prove practical, especially as the lack of rigorous design criteria suggests deformable walls.

For the effuser studies a series of nozzles for different Mach's number were constructed on the assumption that in the narrowest section the velocity would manifest a uniform distribution and be constant in intensity and direction across this section. Hence the first part of the diffuser was designed for a gradual expansion. The pressure measurements actually revealed a shock aft of the narrowest section, whereby the pressure distribution varied from the calculated pressure.

After more exact investigations this phenomenon was attributed to the erroneous assumption of constant velocity in the narrowest section; in fact, several measurements disclosed that the velocities in this section were different on the inside from those on the outside. To remove this

error it was necessary either to modify the nozzle design in the subsonic zone or to allow for the actual pressure distribution in the narrowest section when designing the nozzle profile. The first method was employed in the beginning, and numerous improvements effected with it on the explored nozzles. However, it is thought that better results could be achieved if the velocity distribution in the critical section were being considered. In view of this, experiments have been launched in this direction, although the other method itself had given good results.

Owing to the fact that the most troublesome part of the nozzle is where the walls aft of the critical section are convex, i.e., the part not definitely obtainable by the characteristics method, it was decided to study a nozzle shape suggested by Doctor Gasperi, which did not have this piece and where the gradual expansion aft of the critical section was replaced by an expansion around a corner (fig. 1). This made it possible to design the total effuser by the characteristics method. Such nozzles are much shorter than the others and present no technical difficulties once the velocity distribution in the critical section is known. Experiments are under way with a view to determining a velocity distribution in the critical section according to which the nozzle is then to be constructed. Parallel with supersonic nozzles such nozzles for subsonic velocities were constructed, and of these we shall speak later on along with some results obtained.

Aerodynamic Balance

The design of the balance was governed by three problems:

- 1) Should the whole balance be housed in the low-pressure chamber or not.
- 2) On what principles should the measuring elements be based.
- 3) What decomposition of the aerodynamic forces should be made and what scheme should be followed in the decomposition.

In the preliminary attack of these problems diverse provisory balances were employed with which the determination of only two components of the aerodynamic force was

possible. They did not permit changing of the angle of attack during the tests. (This is the reason the later tests were restricted to the subsonic zone, because there it is at least possible to vary the speed without modification.)

The first types of balances were based on the principle of housing the entire measuring system in the low-pressure chamber of the wind tunnel. The measuring elements were of various kinds. The dynamometric devices used initially were subsequently replaced by fluid capsules of corrugated tubing (reference 1). But the application of such systems was followed by numerous difficulties, especially in the number of necessary calibrations. Even their manufacture was not quite satisfactory, and so their use was only temporary. After other unfruitful attempts it was finally decided to use a double-parallelgram balance with direct reading by weights. An available balance of this kind, used previously in the old wind tunnel of the Air Ministry, was too large for installation in the test chamber and had to be mounted on the outside. The connection between model and balance was similar to that of the other explored balances, i.e., a streamlined spindle. Tightness around the rigid column which transmits the aerodynamic forces from the model to the balance was achieved by means of small corrugated tube compensators. Since some of the tests were carried out with such a balance we shall refer to it again later on. Such a balance made it possible to run tests in the subsonic zone where it frequently is very difficult to make any measurements. But, since interference zones must always be reckoned with in the subsonic range, it was decided to use weights (in the new balance)..

The fact that the carrying of the aerodynamic force to the scale outside of the tunnel disclosed numerous difficulties from the point of view of tightness, while the elastic elements manifested various drawbacks because of the many necessary checks, finally led to the conclusion of designing a balance operating at the same pressure as in the experiment chamber. It was a question of choice of system of transfer of the resultant force from the model to the balance. The decision involved the following considerations: the calibration of the struts and supports at the tunnel speeds in question is extremely difficult and at times, if so-called interference phenomena occur, altogether impossible. Hence it was deemed advisable to reduce such calibrations to a minimum and also to keep

the parts exposed to the windstream to a minimum. The simplest system, therefore, is that which carries the resultant aerodynamic force in its two components outside of the flat tunnel walls, the entire balance being housed in an airtight box. Thus the balance consists of two distinct parts (fig. 2) requiring six elements to define the three principal components (lift, drag, and moment), although the yawing and rolling moment can also be determined. The calibrations are restricted to a minimum.

In fact, if the test specimen is an airfoil reaching from one wall to the other, the model is fastened at the tips, thus exposing it alone to wind in the test chamber. If the model does not span the jet it is anchored by one or two faired supports to a transverse bar equally faired. The fairings turn also when the angle of attack is changed, thus always assuming the direction of minimum drag. These fairings are restricted to a minimum. A large number of fairings were designed for different models and speeds.

In the decomposition of the force into two components two methods were employed: one permitting the exact measurement of lift and moment of bodies having a small lift (shaded scheme, fig. 3). For this no fixed points are necessary, which, moreover, would be difficult to realize in view of the severe temperature changes to which the metal casing is exposed. The other, the orthodox method is used for lifting models. The system of angle-of-attack change was designed with great care; its operation is such that one drive permits the rotation of the graduated sectors to which the model is attached. The measuring elements (figs. 4 and 5) consist of sliding weights operated by small d.c. motors. The latter can be controlled by the element itself by leaving its position of equilibrium or in case of severe oscillations of the element by the operator from the outside. The sliding weight affords a balance up to 10 kilograms and, after addition of two weights from the outside, to 30 kilograms. The system of automatic contacts and clamping controls, as well as for adding of the two weights, is illustrated in figure 6, the whole being enclosed in a strong, easily removable box which permits a quick mounting and, if necessary, inspection. The measurements are read from the weights through the window.

Optical Equipment

The supersonic tunnel is to be provided with "striometric" and "interferometrical" equipment. The first is under construction, the second still in the design stage, since it is intended to try out the striometric equipment first and to utilize the data for the design of the other, which, according to the National Optical Institute at Florence presents some difficulties, especially in overcoming the vibrations of the tunnel during operation. The tunnel is of all-metal construction and rigidly coupled to the compressor and the d.c. motor. It is also known that such vibrations even of minimum amplitude may create considerable interference especially in the interferometric observations. Originally it was intended to support the entire optical equipment on a beam with separate foundation. This would have stopped the vibrations, but then the question arose of how to mount the model so as to free it too from the tunnel vibrations. This solution, though feasible, proved very complicated. Hence it was preferred to attach both the optical equipment and the model rigidly to the tunnel. In fact, if the supporting base is robust and the equipment light and compact, the whole - model and optical equipment - rigidly fixed to the tunnel, must vibrate in synchronism, so that all relative motions between the two elements disappear and so assure satisfactory operation. The result is the set-up shown in figure 7. The two lenses L_1 , L_2 of 350 millimeters diameter and 1 meter focal length are rigidly mounted and disposed to form a continuation of the metal wall, thus avoiding local interference as well as assuring tightness. Since the lenses must withstand pressures up to 4 atmospheres, they must be quite thick. As regards the light source two solutions are provided: the normal incandescent and the mercury lamp. Micrometer screws assure proper adjustment, while rigidity guarantees ease of operation without extensive readjustments.

PART II

EXPERIMENTAL RESULTS

Parallel with the preliminary studies for the design of the experimental equipment, some subsonic experiments were carried out, parts of which had been reported at the A.I.D.A. meeting in Naples, May 1938, but had never been made public. In view of the close relationship with the

other part of the experiments I shall quote the most important facts.

Preliminary Remarks

The most difficult task in the subsonic tests is the method of conducting the experiments, or more precisely, the method by which the test chamber must be built. In point of fact it is very difficult in this zone to realize, because of the usually small tunnel dimensions, a flow which assures that the produced aerodynamic phenomena are similar to those visualized if the body moves at the same speed in static flow.

In a flow between rigid walls where the effective section of the test chamber becomes smaller than the preceding sections because of the airfoil, the thickness of the experimental body causes a velocity increase over the entire section in the subsonic zone, which alters the aerodynamic phenomena with respect to those which are formed if the body moves in an infinite fluid.

Such alteration may become quite considerable if the airfoil thickness is great compared to the section of the test chamber and the speed approaches velocity of sound. This is readily seen from figure 8 where the Mach figures (M_2) occurring at the maximum airfoil thickness are plotted against the Mach figures (M_1) existing close to the wing leading edge. The graphical results were computed with sole consideration to the velocity variation resulting from the sectional change because of the presence of the airfoil, independent of the aerodynamic behavior of the airfoil itself, proceeding from the assumption of adiabatic expansion and constant velocity across the whole section. Various values of the maximum airfoil thickness were considered which were given in percent of the diameter of the assumedly circular tunnel section. The cross-sectional change which is more pronounced when the airfoil assumes a setting relative to the flow, varies in the two parts into which the airfoil divides the chamber, thus creating greatly unlike velocity gradients on the upper and lower surface of the airfoil section. This drawback could be largely removed by an open jet surrounded by a static air mass, but if the aerodynamic phenomenon is not localized and if it influences appreciably the outer layers of the flow as well it is to be borne in mind that the effect of the static air around the flow on the outer layers will be different from that of a motion with the same velocity as

the flow and that the aerodynamic behavior of the body is far from that desired and the phenomena may as a result be very different in the wind tunnel than in reality.

However, it may be assumed that the substitution of the layers surrounding the flow by layers of infinite inertia as exemplified in the case of the jet being conveyed by rigid walls, will involve greater discrepancies from the actual case than by replacement with layers of zero inertia as with the open jet, especially if the dimensions of the airfoil section are reduced to the necessary minimum. For this reason the second method is preferred for the execution of the tests; both constructed tunnels have an open section for measuring the forces and pressures.

Description and Characteristics of the Subsonic Tunnels

The two tunnels differ only in size. The first in which the force measurements were made is the smaller. Their general characteristics are as follows:

1) They have a rectangular rather than circular section. Hence it is possible to obtain a uniform flow over the whole length of the airfoil, which would be more difficult to obtain in a circular tunnel, especially if the airfoil spans the jet and the dimensions are quite large.

2) Its design can be seen from figure 9: It comprises a front portion with a nozzle designed to minimize the interferences due to the centrifugal force. The nozzle terminates abruptly. The subsequent part of the tunnel consists of two flat, parallel walls with greater distance than the channel section at the nozzle end and two upright walls, so that the motion of the air may be considered plane. The first tunnel has a jet of $40 \times 28 \text{ cm}^2$ section; the first dimension represents the distance between the upright walls and is equal to the explored wing span; the jet of the second is $40 \times 50 \text{ cm}^2$. Before proceeding to the actual tests, the jet uniformity was ascertained. The static pressure was determined along the three principal axes, horizontal, vertical, and transversal. Several records are shown in figures 10, 11, and 12. The ratios: dynamic pressure upstream from the nozzle to static pressure reading are shown for the different positions, from which the Mach number can be deduced. On this occasion the dynamic pressure in the test chamber was determined at different Mach numbers. Such a determination, extended to

nearly $M = 1$ indicated that the dynamic pressure in the test chamber was practically always equal to the dynamic pressure upstream, where the flow velocity is known to be small. This proved that adiabatic transformations took place in the tunnel, and that the calibration formula of the Pitot tube is an accurate check on the accuracy in the sonic field. Some readings are reproduced in figure 10, the small circles indicating the dynamic pressure in the test chamber, and the horizontal line the dynamic pressure upstream from the nozzle. Following these investigations the model experiments were launched, while verifying that the dynamic pressure at the edges of the field was not affected by aerodynamic phenomena created by the wing, and that the static pressure in tunnel-axis direction retained a constant value between two sections directly upstream and downstream from the wing. In the determination of the forces, effected on a model of 40-millimeter chord in the nozzle 280 millimeters high, the recorded static pressure was not perceptibly affected by aerodynamic phenomena, up to speeds closely approaching velocity of sound. In the pressure measurements made on an airfoil of 90-millimeter chord the use of the 280-millimeter nozzle necessitated restriction to the range below $M = 0.8$, since with the 500-millimeter nozzle a speed equal to 0.9 that of the velocity of sound was no longer obtainable without sacrificing pressure uniformity.

Test Procedure

With the described tunnels the lift and drag coefficients of an airfoil (fig. 13) were recorded at different speeds and angles of attack. The airfoil really was a propeller profile, used in the Italian Air Service, hence the pressure distribution was also studied. For the force measurements the dimensions were: 40 mm chord, 2.5 mm thickness. Such dimensions are structurally least desirable, and it was purposely intended to make the dimensions as small as possible in order to reduce scale effect. The model consisted of a thin steel plate and proved satisfactory, except at high speeds and high angles of attack where the outer edges manifested a slight curvature. This airfoil was studied in the original subsonic tunnel and is to be checked in the second tunnel, for purposes of comparison and scale effect. The forces were measured with a two-parallelgram balance (fig. 9). The airfoil was mounted on two arms a which permit changing of the angle of attack when at rest. Two streamlined struts b anchored the

arms a rigidly to a frame c, which extends beyond the tunnel and terminates at the balance. The latter is supported on knife edges. Lift and drag were measured successively by blocking either one of the parallelograms, with the help of the diagonal d.

Tightness around the arm c was achieved with an elastic body cm, fastened at one side to the tunnel, on the other to the balance.

To eliminate the tare caused by the pressure on it, a symmetrically similar body cm' served as compensation. Before and after every test the pressure equilization between the two elastic bodies was checked, even at very high vacuum.

The elastic body cm produced a negligible insensitivity in the drag tests. All supporting arms were faired in and the tare was of the order of 1/5 of the minimum drag. The airfoil used in the pressure tests was of steel, had a chord of 90 millimeters and was fitted with 1-millimeter pressure-orifice tubes. The wing tips were attached to metal disks themselves fastened to the tunnel walls, and permitted changing of the angle of attack by rotation. The pressure leads terminated at a multiple manometer, the measurements were photographically recorded.

The Reynolds Numbers in the force measurements ranged around 180,000, with some fluctuations, since the tests were made at different speeds and constant angle of attack. The tests were repeated several times, even at larger Reynolds Number (up to 250,000 at low angle of attack). Now appreciable differences were noticed.

The pressure measurements were made at much larger Reynolds Numbers (500,000). The air speed was computed from the pressure, on the basis of an assumedly adiabatic expansion.

Provisory equipment operating on the Schlieren method was used. Various records are shown in figure 18 to 22. Being of a temporary nature and quite difficult to handle, these records leave much to be desired. But in the study of the various phenomena they proved practical.

Force Data

The results are reproduced in figure 14 to 17. They disclose the following:

- 1) The lift computed with the formula $c_a = \frac{A}{\rho F V^2}$ increases at equal angle of attack with the Mach number. Up to a certain M it is very similar to Prandtl's and Glauert's theoretical value, (fig. 14).
- 2) The Mach number at which c_a departs from theory decreases in accord with the predictions for increasing incidence with respect to the wind direction (see Pistolesi, Volta meeting, Rome, 1935).
- 3) At very high angles of attack approaching stall in the normal speed range, figures 14 and 15 disclose the lift to decrease at relatively low Mach numbers, thus confirming the prediction of decreasing $c_{a_{max}}$ as well as of the corresponding critical angle of attack at increasing Mach number.
- 4) Following the departure of the c_a curves from that predicted by Prandtl and Glauert, they reach a maximum, after which the c_a values decrease (fig. 14). After c_a has dropped a certain amount the airfoil manifests oscillations as the speed is increased: the aerodynamic forces fluctuated at a rate which made measurement impossible. At still higher speed the field of instability is exceeded and the oscillations cease. Then the c_a values are high again, especially at high angles of attack. These values remain approximately constant almost up to sonic velocity (fig. 14).
- 5) Up to Mach numbers of around $M = 0.6$ the angle of attack for zero lift remains unchanged and $\frac{d c_a}{d \alpha}$ increases up to a Mach number between 0.7 and 0.8, as envisioned.
- 6) At large M the maximum lift is not reached within the explored zone (figs. 15 and 16). This unexpected phenomenon seems at least strange, but additional confirmation is necessary even if optical observation suggests various explanations.

7) The maximum efficiency of the airfoil (fig. 16) increases with increasing Mach number, becoming maximum at between $M = 0.5$ and 0.6 followed by a quick drop. There is an appreciable drop when M exceeds 0.8 .

8) The c_w curve (fig. 17) corresponds to the c_a curve. One noteworthy feature is that a temporarily flat distance is followed by a zone of gradually increasing c_w without manifesting the marked increment found elsewhere at $M = 0.8$, spoken of as a regular sound barrier. In the oscillation zone the c_w value rises considerably at high angle of attack and then remains constant. At small setting this increment is less and at low angles of incidence the c_w curve is quantitatively in agreement with that obtained for similar airfoils in propeller experiments (see Douglas, Volta meeting, Rome 1935).

9) The drag increment (fig. 16) due to the rise in Mach number is almost constant and, at not too high c_a values, independent of c_a and hence of the setting.

Optical Test Data

Concurrently with the force measurements, we made some optical observations. The results are as follows:

1) To the Mach number at which the c_a curve diverges sensibly from the theoretical curve corresponds the appearance of the first shock wave on the upper surface of the airfoil (fig. 18).

If the angle of attack is small the shock wave on the upper surface corresponds to one on the lower surface slightly farther back than the first.

2) As the speed increases the wave is extended and becomes more accentuated. Under suitable illumination it disclosed the formation of a kind of wake zone directly behind the wave on the upper surface immediately behind the shock wave itself (fig. 19).

3) Raising the Mach Number still more after the first shock wave has reached considerable dimensions and moved somewhat to the rear, a second shock wave can be plainly observed at increasing speed. This wave does not reach to the upper surface but ends where it meets the vortex zone created by the first shock wave (fig. 20).

4) At still higher speeds the first wave lengthens out and inclines, the second tends to advance with the result that both meet in a certain point (fig. 21).

At this speed the oscillations distinctly visible optically, begin. The first wave oscillates and tends rearward while the second advances from its original position toward the first.

5) As soon as the oscillation zone is passed the two shock waves meet and separate, the first wave settles first, while the second still oscillates for a certain time. The first wave moves backward quite considerably and is notably inclined. Its extension is much increased. The second wave has also moved backward to the extent of exceeding the trailing edge of the profile. Aside from these two shock waves on the upper surface there appears very distinctly a third wave on the bottom surface in corresponding position to the second wave on the upper surface (figs. 22a, 22b, 22c).

Discussion Based on Optical Observations

The optical observations, together with the previous findings, prompted the desire to establish a logical relationship between the different phenomena with a view to finding the causes back of them. A feasible explanation is as follows:

As soon as, through the expansion on the front of the upper surface the sonic velocity is locally reached or exceeded, the successive recompression occurs suddenly through a compression shock. The region of exceeded sonic velocity being initially small this wave is scarcely visible. The wave is not normal to the profile, hence the shock is oblique, causing behind the shock an upward deflection of the velocity, which in turn tends to produce a break-away of the flow from the profile, which is optically visible. This deflection is very small at first, since the velocity before the shock is not much in excess of the velocity of sound, so that the shock wave has but little inclination and the disturbance created by the separation is small. After the shock, subsonic velocity reigns again, hence the successive divergence of the fluid filaments in the rear part of the upper surface produces a recompression.

With increasing Mach number the original velocity of the shock and the wave inclination and hence the separation

increase. The lift coefficient decreases, the drag coefficient increases. At further increasing Mach number the pressure increment of the shock increases as a result of the speed increase before it, the shock wave inclines more and more until finally the speed after the shock can reach or exceed the local velocity of sound.

At this point the phenomenon changes suddenly: The divergence of the fluid filaments produces expansion instead of recompression, being in the supersonic field; there is a new increment of velocity lasting to the divergence of the stream filaments and incipient recompression, where necessarily a second compression shock occurs.

At still further increase in speed the rise of the velocity deflection relative to the direction before the shock reduces the filament divergence, the expansion is less extensive and recompression sets in sooner. The second shock wave tends to approach the first which already manifests a marked inclination, hence gradually drift apart. Then the oscillations of both shock waves begin and, in correspondence with them, the aerodynamic forces. The cause of this phenomenon has escaped us entirely. The forward wave moves toward the back while the rear wave, which is now partially joined with it, moves forward.

Increasing the speed, the oscillations of the two waves increase because the mutual interference increases up to a certain point where they die out when both waves, having then increased considerably, no longer meet because of their inclination. The first shock wave has moved much farther backward and the second compression shock starts only at the trailing edge. Correspondingly, there is a wave on the lower surface emanating from the wake.

It is readily apparent that such a disposition of the waves favors the low pressure on the suction side, since, first, the low pressure field before the first shock increases, and, second, the expansion after the shock is augmented. In fact, the movement of the first wave toward a point aft of the maximum airfoil thickness where the velocity before the shock already diverges considerably from the direction of undisturbed flow has the effect of a subsisting divergence even after the shock, despite the reduced deflection during the shock, and so points to a marked increase in velocity. The appearance of the shock on the lower surface of the wing suggests the existence of a low-pressure zone toward the trailing edge, capable of accelerating the flow.

According to the Schlieren photographs, the phenomenon may be briefly explained as follows:

Following the first shock a vortex zone with low velocity but low pressure is formed on the upper surface of the wing, since the flow outside of this zone has undergone a severe expansion. The pressure in proximity of the trailing edge is therefore lower than on the bottom surface of the wing. As soon as the air, coming from the bottom surface, combines again with that from the upper surface where the pressure is lower, a pressure equalization is to be counted on, hence the air from the lower surface of the wing must expand, that from the upper surface, compress.

The flow on the lower surface thus expands in proximity of the trailing edge and exceeds during the expansion with its speed the velocity of sound, in addition to being deflected upward. Hereby, however, it encounters the flow of the upper surface which has a different speed. At this instant the pressures, as well as the directions of the two flows, must be identical; both must deflect alike. But the deflection and the pressure equalization of two such supersonic flows can be effected only by two shock waves emanating from the point of contact, as it actually occurs at the trailing edge.

Results of Pressure Measurements

In order to determine the various aerodynamic phenomena and to check the different assumptions formulated the pressure distribution on the top and bottom surfaces of the same airfoil section was explored at different angles of attack and speeds. For a qualitative appraisal of the effect of tunnel dimensions on the test data the same airfoil section was tested in jets of different length. The tests were made first in the smallest, then in the largest tunnel (50 x 40 cm² test section). With the latter two series of tests were made for different settings. In the first series the jet behind the nozzle emptied into a chamber 62 cm high, in the second, 74 cm high. The object was to ascertain if and to what extent the dimensions of the air layer enveloping the current on both sides affected the test data.

These experiments disclosed that, so long as the static pressure measured at sides of the flow is constant in

two sections of equal distance upstream and downstream from the wing, the results are practically unchanged irrespective of the dimensions of the dead air space. But as soon as the aerodynamic phenomena make themselves felt at the periphery of the current the results obtained change considerably for each set-up. The Mach number obtainable under these conditions can be raised only through greater tunnel height, thus involving tunnels of notable height at high Mach numbers. Below this admissible M the size of the dead air space in which the air jet empties has no appreciable effect on the test data, but much on the uniformity of flow and on the pressure along the tunnel axis. From the numerous measurements, we have selected those for 1° and 6° angle of attack and 50×40 cm² test section, and the results of two test series for 6° angle of attack, one with the 28×40 cm² nozzle, the other with the same nozzle but 72 cm high test chamber.

All these experiments were made with control of the pressure at the periphery and interrupted as soon as the pressure changed. The diagrams give the pressure differences between the pressure in the test chamber and that recorded at the different points on the upper surface of the airfoil. These pressure differences were then divided by the dynamic pressure

$$q = \frac{1}{2} \rho v^2$$

so that the ordinates present these ratios instead of the dimensional quantities. Each plot gives, aside from the angle of attack and the Mach number, the data for q = dynamic pressure in the test chamber, p_1 = static pressure upstream from the tunnel nozzle, p_2 = static pressure in the test chamber and the lift coefficient c_a obtained from integration of the area of the diagram. The pressures were read in mm Hg. Figures 23 to 29 show these pressure diagrams for $\alpha = 1^\circ, 5.30^\circ, 6^\circ, 6.30^\circ$. The diagrams for $\alpha = 6.30^\circ$ give the results obtained with the 50×40 cm² nozzle and the 72 cm high test chamber.

From these diagrams and others not reproduced, the following conclusions can be drawn:

- 1) At low speeds up to where the first compression shock occurs the pressure distribution is in good agreement with Prandtl's and Glauert's theoretical data indicated with dashed lines. On the whole, the differences are

confined to the high pressure zone where the theoretical exceed the experimental values.

2) As soon as the local velocity of sound is exceeded as a result of the low pressure the successive recompression occurs through a compression shock, which causes a substantial change in the pressure distribution. Actually the expansion is little accentuated before the shock, and quite gradual at higher Mach numbers. After the shock the low pressure over a certain distance discloses a progressively decreasing aspect and then drops quickly and considerably; a thick boundary layer appears to form which is probably attributable to the deflection of flow due to shock.

3) At increasing speed the shock has a tendency to move backward. The forward low pressure decreases still more. After the shock the low pressure is smaller and maintains the previously described course, although the recompression after the initial distance is less severe. Then a slight low pressure starts on the lower surface near the trailing edge due to the fact that the flow coming from the upper surface is in upward direction and causes an acceleration of the flow coming from the lower surface. The drop in low pressure on the leading edge and the smaller extent in this part of the diagram of the low-pressure zone seems quite logical and readily understandable.

A cursory consideration discloses the following: At the point where the low pressure forms and a positive pressure gradient results, an increment of velocity must be counted on. This can be ascribed, at the normal speeds, to the convergence of the stream filaments. Where this convergence stops the low pressure is maximum and the speed reaches its maximum value, then the recompression starts. In the sonic field this filament convergence is so much less effective as the Mach number is larger. In any case the sonic velocity cannot be exceeded in the convergent part; at small Mach number the speed increase and hence the pressure decrease obtainable in such a zone is great. But at very high Mach number the sonic velocity is soon reached, so that both the speed and the pressure gradient will be small. Naturally, the sonic velocity can be exceeded in the following divergent part and hence cause an expansion which terminates in a compression shock.

To verify this explanation the points at which sonic velocity was reached in the different diagrams were checked

on the $6^{\circ}30'$ angle-of-attack test series (adiabatic expansion being assumed). It was found that sonic velocity was very approximately reached at the points of maximum depression at low speed (shown as small rings). The choice of the test series for $\alpha = 6^{\circ}30'$ was due to the fact that it offered the greatest number of test points in that particular zone.

4) If the speed is increased further supersonic velocity reigns even after the shock. Then the conditions change because the flow filament divergence after the first shock is followed by a further expansion associated with a marked increment of speed. We are again in a supersonic field and recompression is contingent upon a second compression shock. After the second shock, the low pressure is still appreciable, hence the expansion of the pressure-side flow near the trailing edge more accentuated. With low pressure on the suction side the lift coefficient itself increases. The c_a curve again rises in function of the Mach number, hence must disclose a minimum at the beginning of the formation of a second shock wave.

5) It was found that as the Mach number increases the low pressure in proximity of the leading edge decreases while at the same time the low pressure in the median zone becomes greater. At high Mach numbers the low pressure increases in proximity of the trailing edge as soon as the second shock wave occurs. For this reason the center of pressure of the airfoil moves considerably backward, and the wing moment with respect to the leading edge increases with increasing speed.

6) The integration of the pressure area diagrams obtained by approximation and giving the c_a values shown plotted against the Mach number are in close agreement with the data from the force measurements (fig. 30).

Such accord of test data seems quite remarkable, since it removes many doubts which could be raised if the obtained results had been contingent upon one or the other of the test methods employed. In point of fact the entire experimental arrangement had been modified when changing from the force to the pressure measurements including the ratio of tunnel dimensions to model dimensions and the Reynolds Number without the results disclosing fundamental discrepancies. This fact lets us hope that our test method will lead to practical results and induces us to continue this line of attack.

Admittedly, much remains to be done as regards experimental method and experimental accuracy. It is hoped to supplement the first experimental results by other more accurate and detailed test data within the near future, permitting us to establish a criterion for the relationship existing between profile form and profile characteristics, so as to make available those factors essential for the progress of modern aviation.

Translation by J. Vanier,
National Advisory Committee
for Aeronautics.

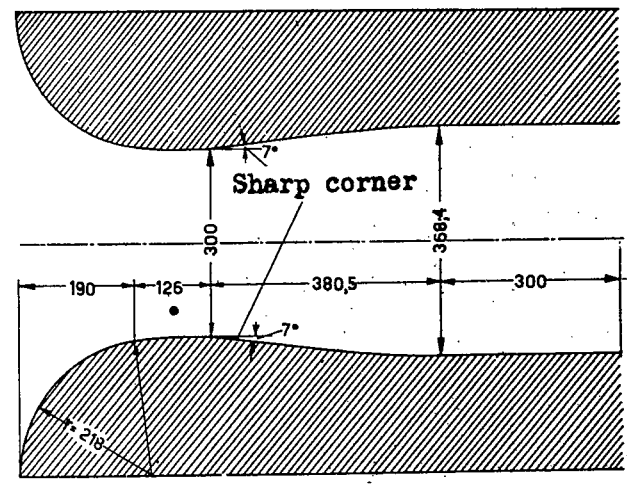
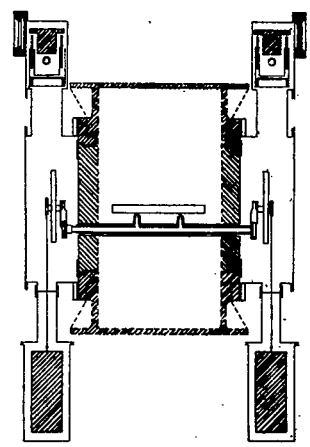


Figure 1.

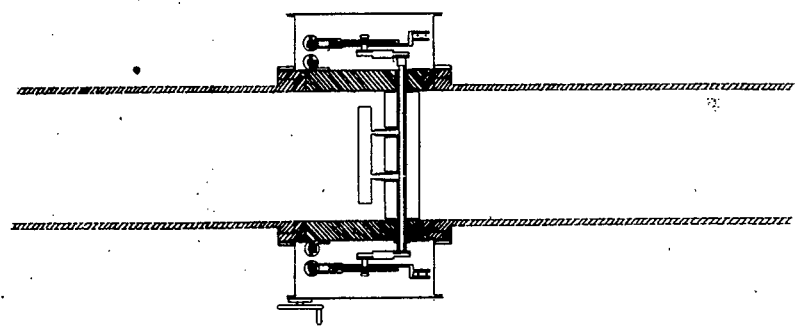
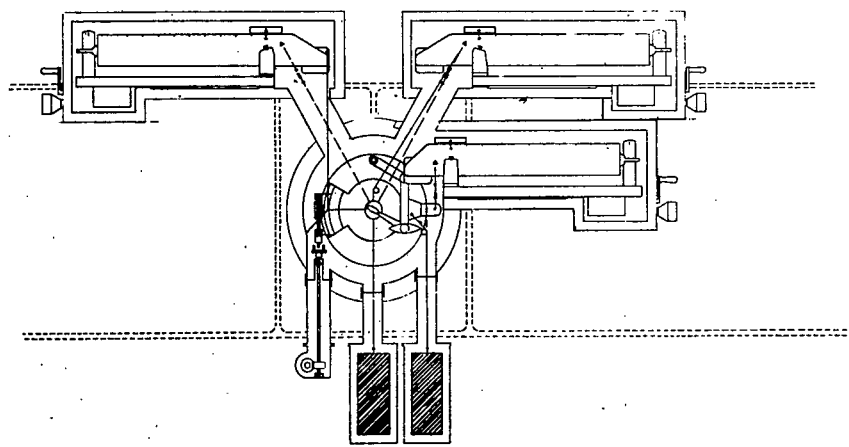


Figure 2.- Aerodynamic balance

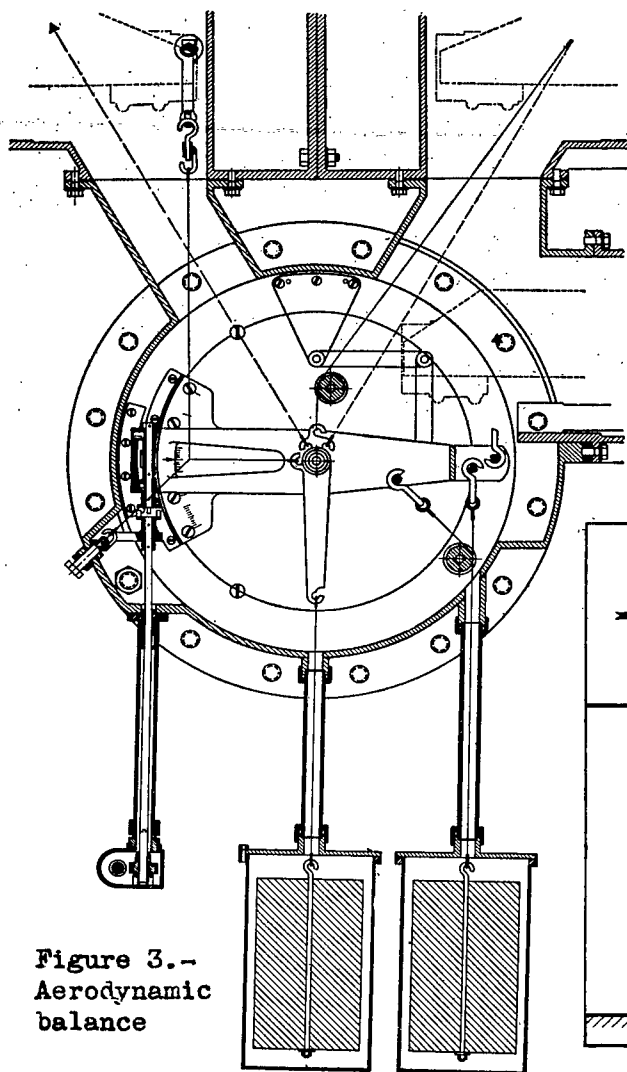


Figure 3.-
Aerodynamic
balance

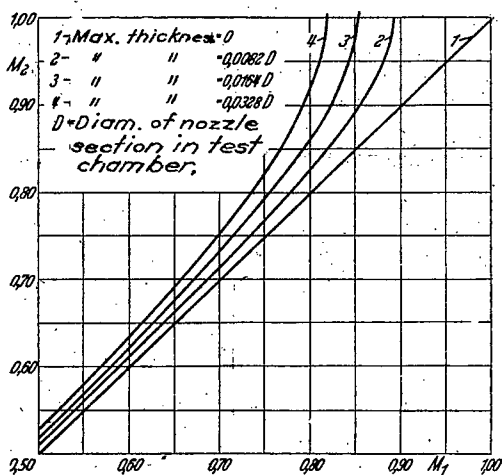


Figure 8.

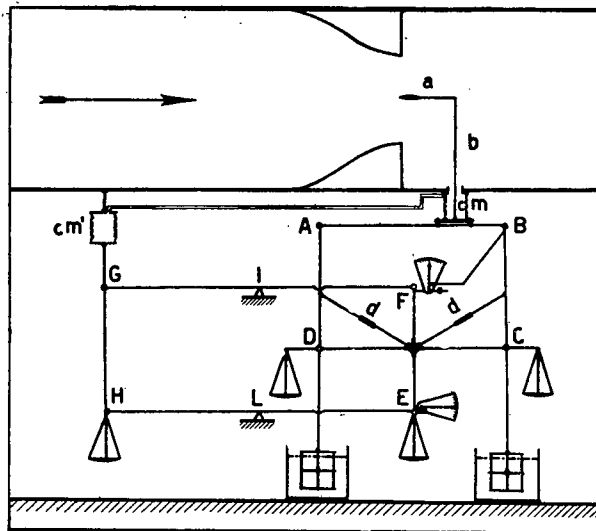


Figure 9.

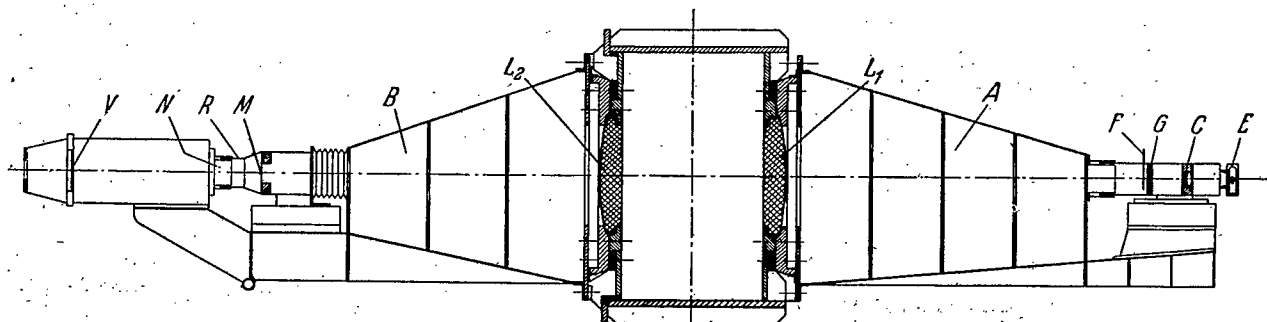


Figure 7.- Schlieren method.

- | | |
|---|-----------------------------------|
| L ₁ L ₂ Flat hyperbolic lenses. | V Opaque disk. |
| A B Supporting frame. | F Adjustable slot. |
| N Light screen . | G Filter for monochromatic light. |
| R Extension tube. | C Condenser. |
| M Schlieren diaphragm. | E Light source. |

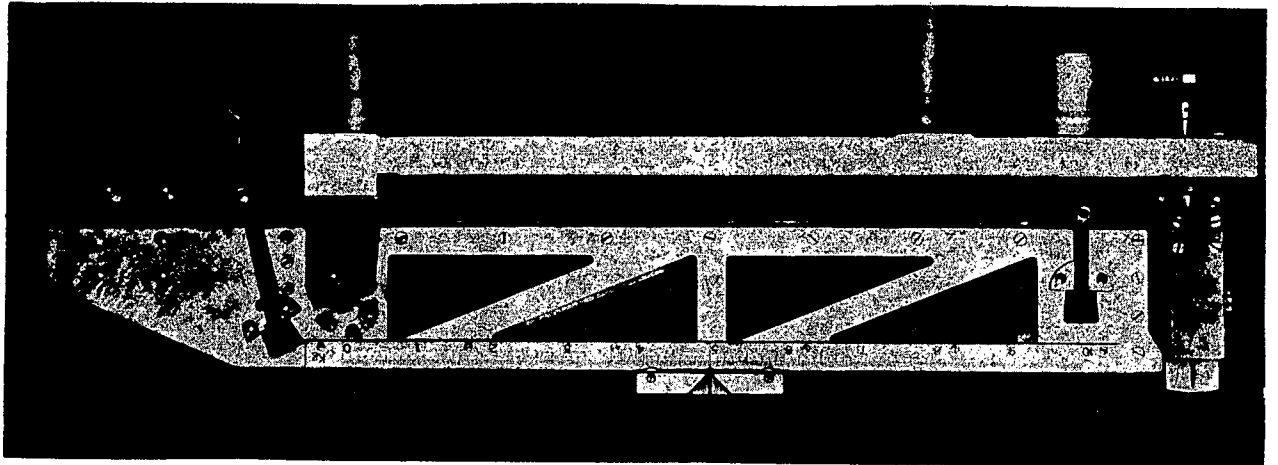


Figure 4.

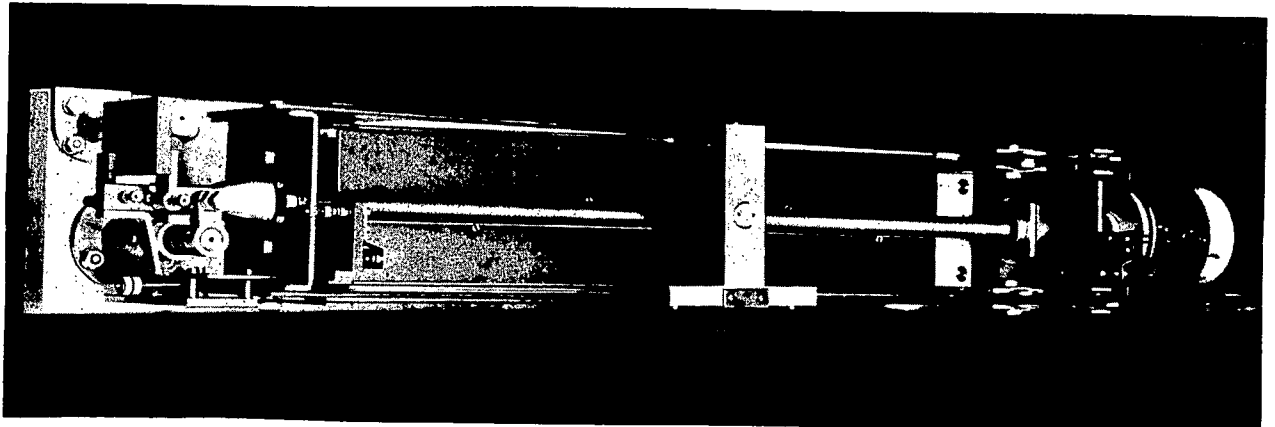


Figure 5.

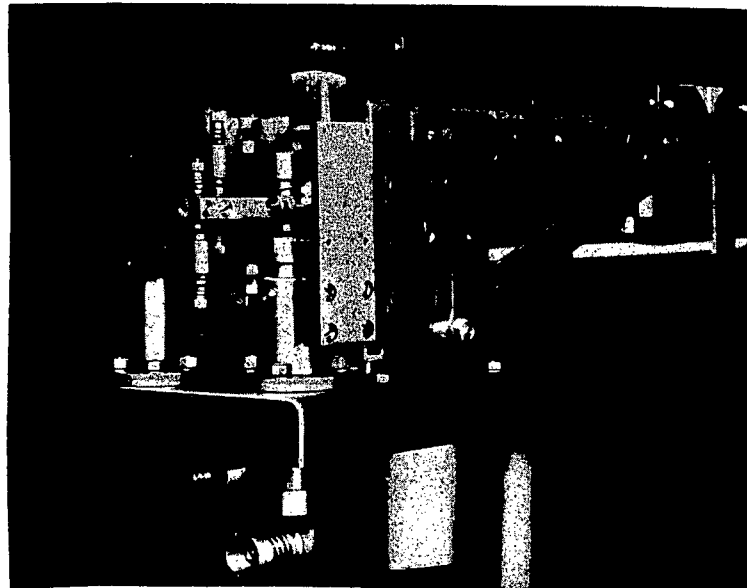


Figure 6.

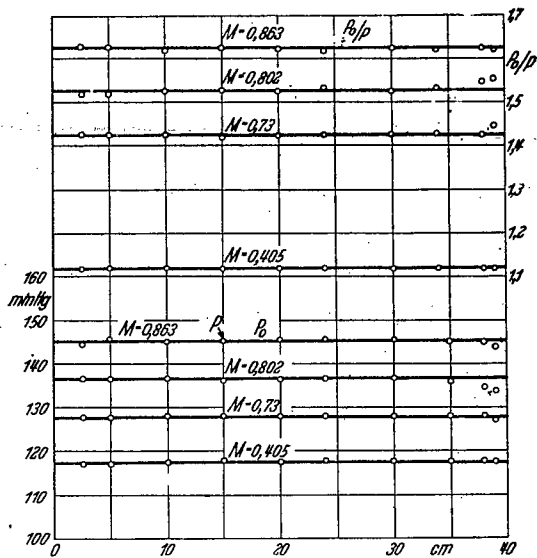


Figure 10.

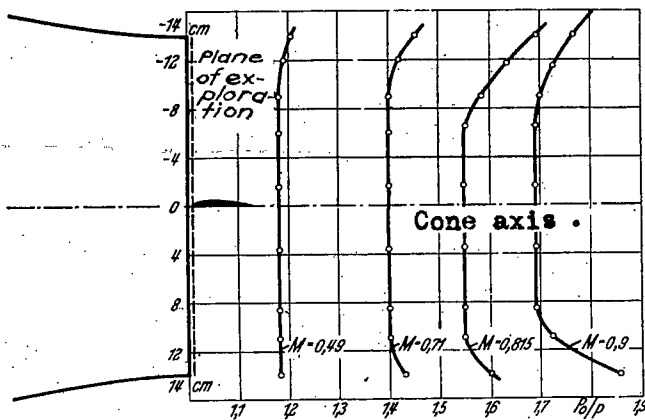


Figure 11.

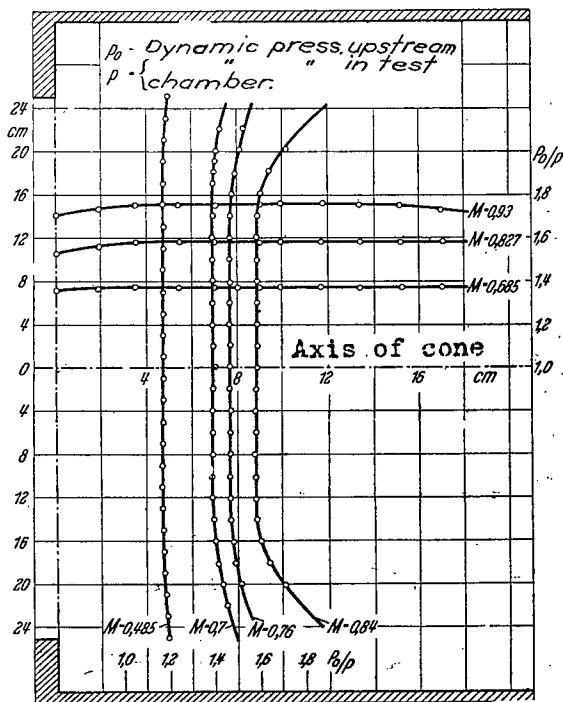
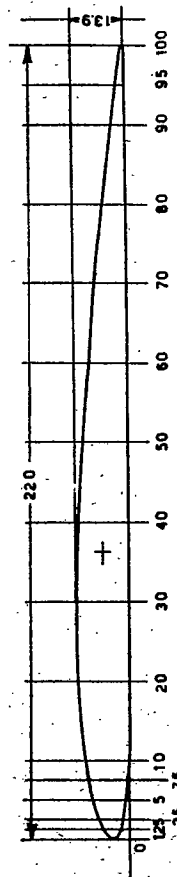


Figure 12.



Abscissa in % of wing chord

X	0	1.25	2.50	5.0	7.5	10	20	30	40	50	60	70	80	90	95	100
y_1	2	3.2	3.8	4.55	5.05	5.4	6.2	6.32	6.0	5.52	4.85	3.97	2.92	1.75	1.05	0.2
y_2	2	1.12	0.87	0.55	0.30	0.15	0	0	0	0	0	0	0	0	0	0.10

Figure 13.- Airfoil A

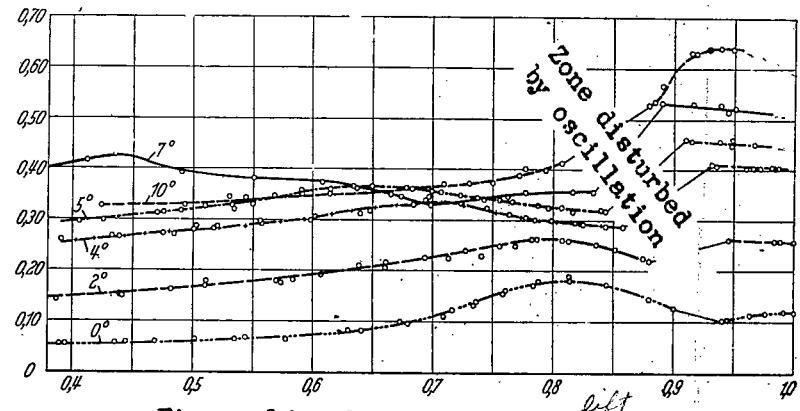


Figure 14.- Coefficient of strength.

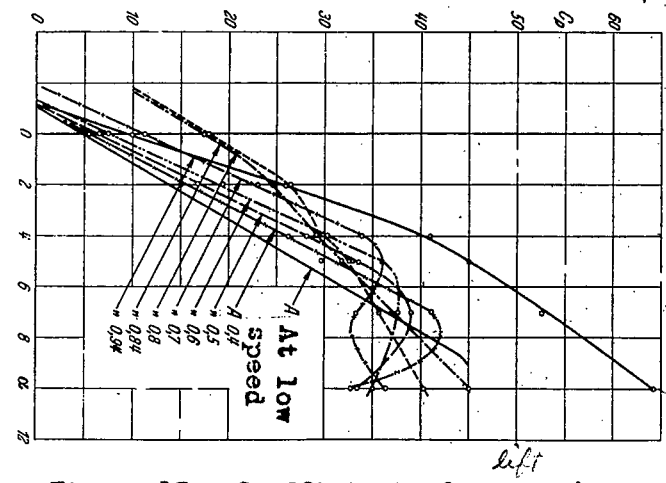


Figure 15.- Coefficient of strength.

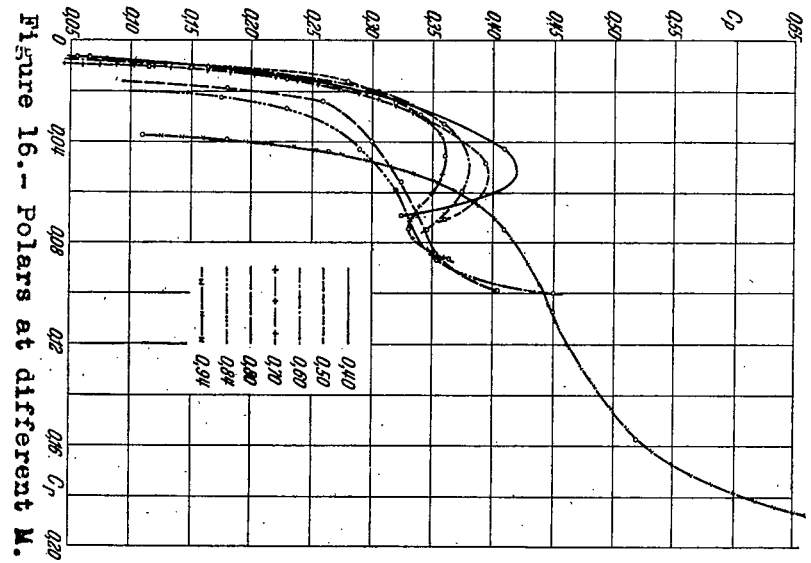


Figure 16.- Polars at different M.

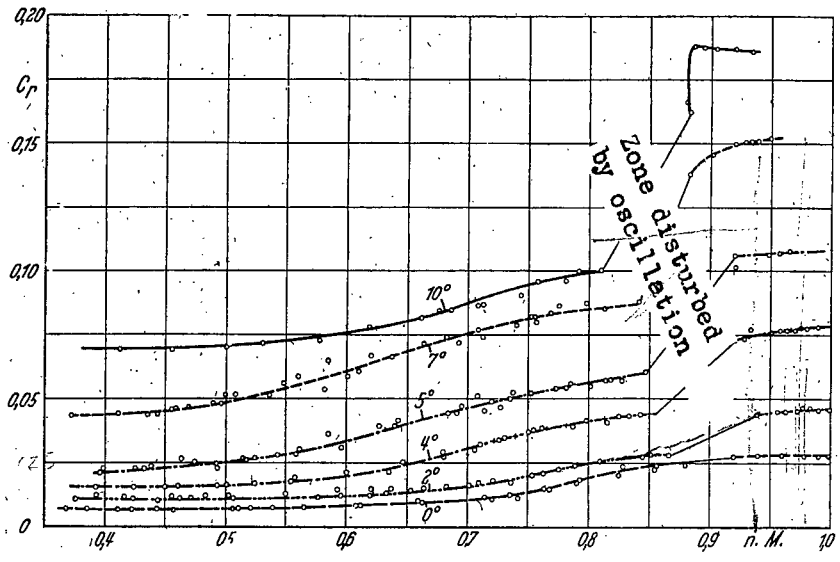


Figure 17.- Coefficient of resistance.



Figure 18.



Figure 22a.



Figure 22b.



Figure 22c

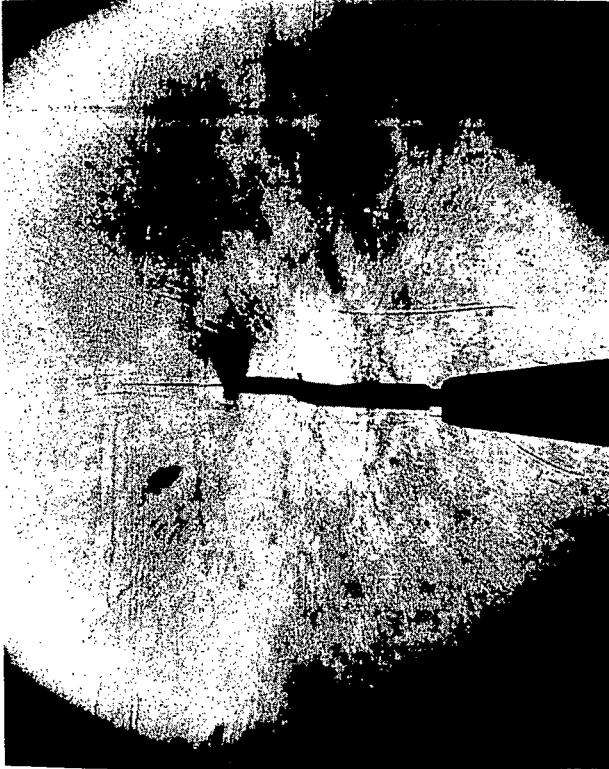


Figure 19a.

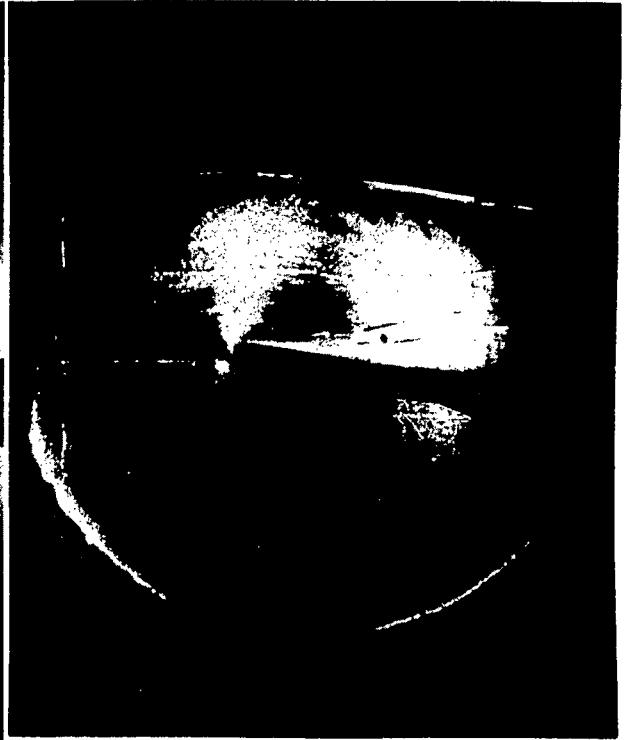


Figure 19b.



Figure 20a.

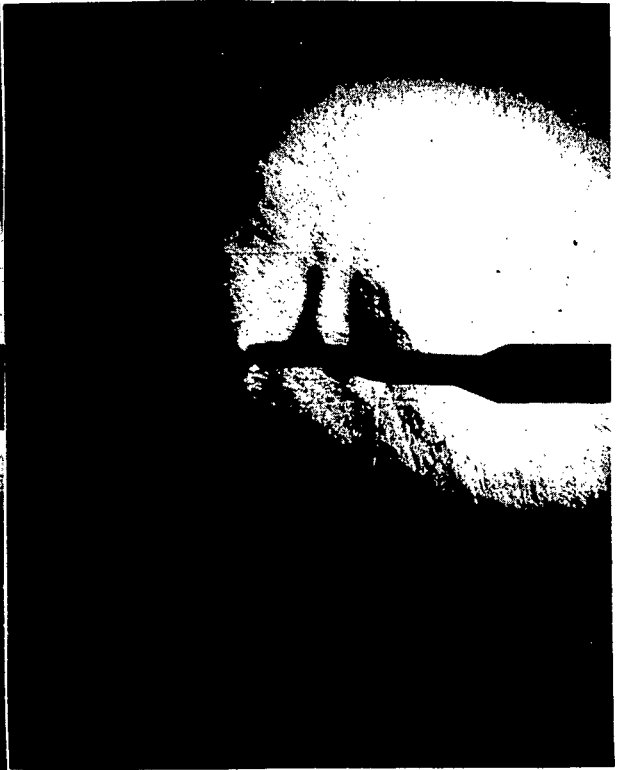


Figure 20b.

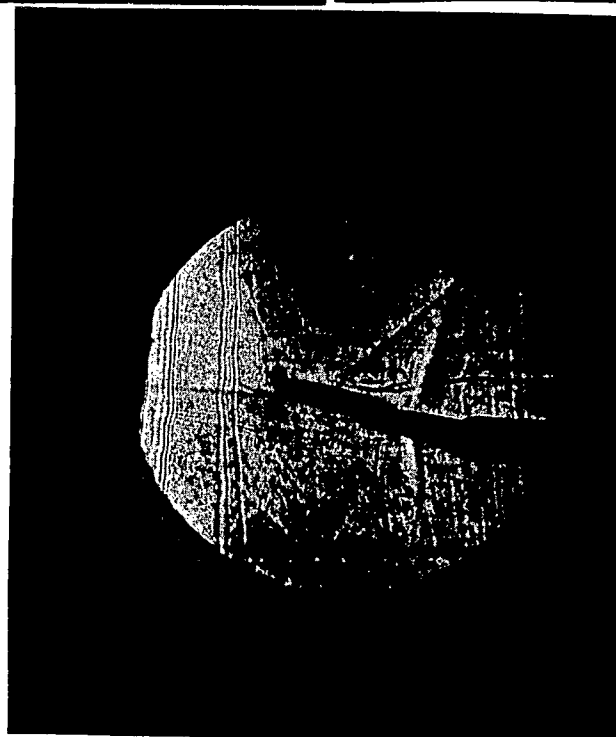


Figure 21

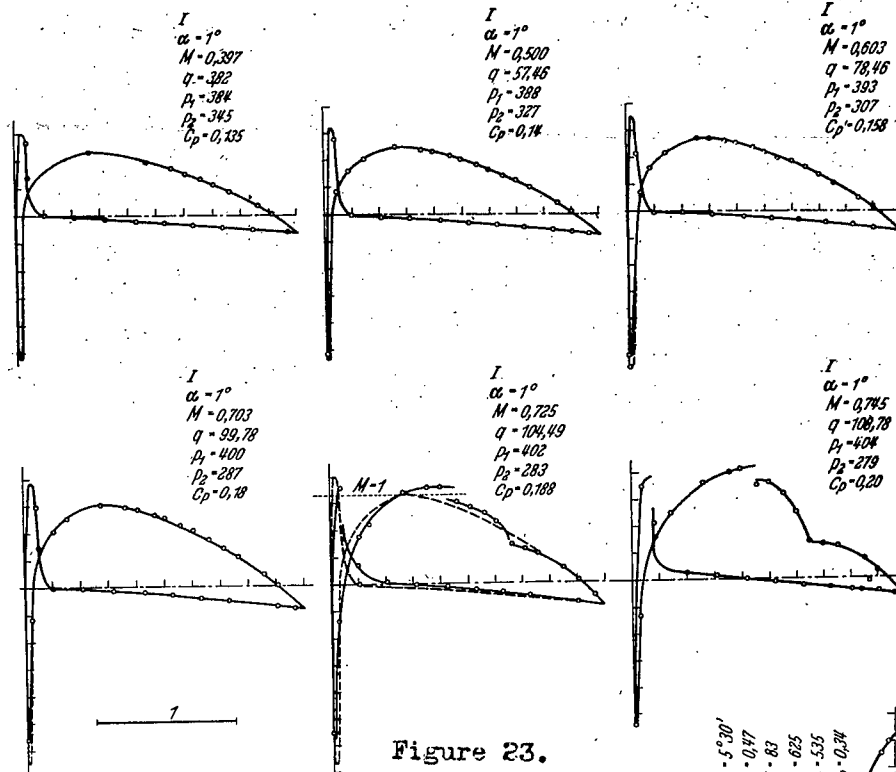


Figure 23.

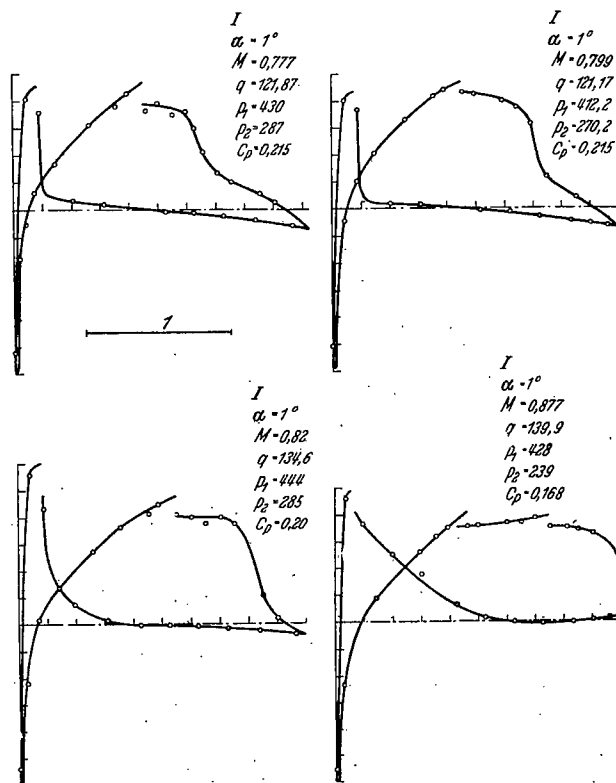


Figure 24.

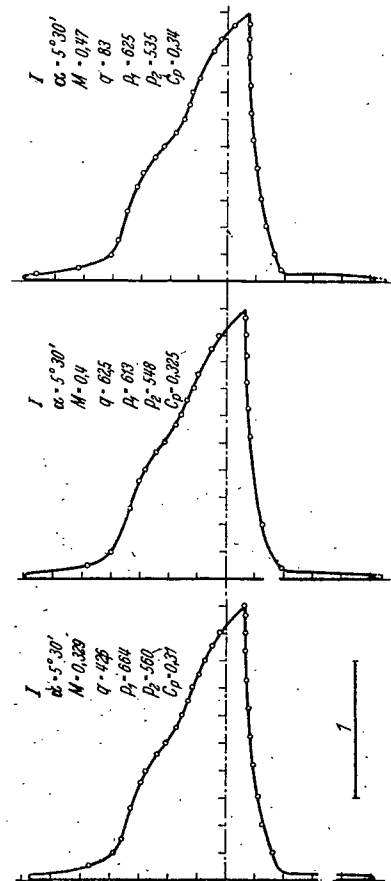


Figure 25.

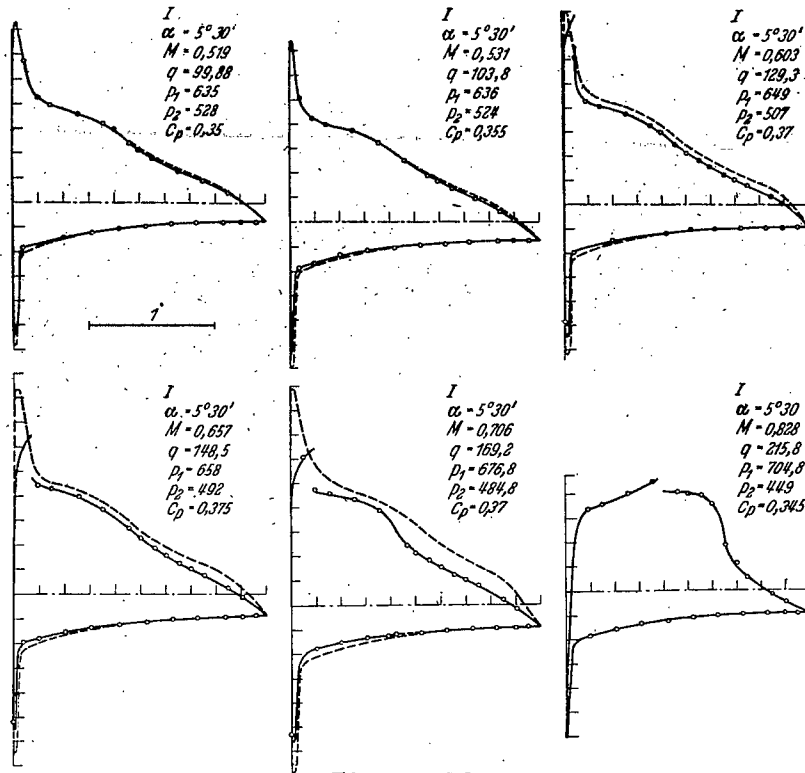


Figure 26.

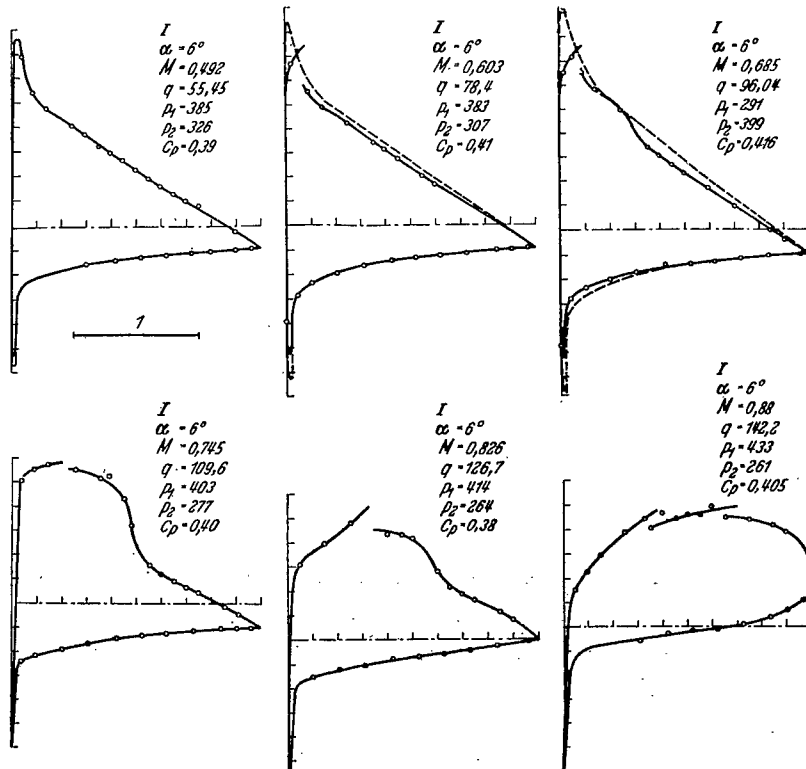


Figure 27.

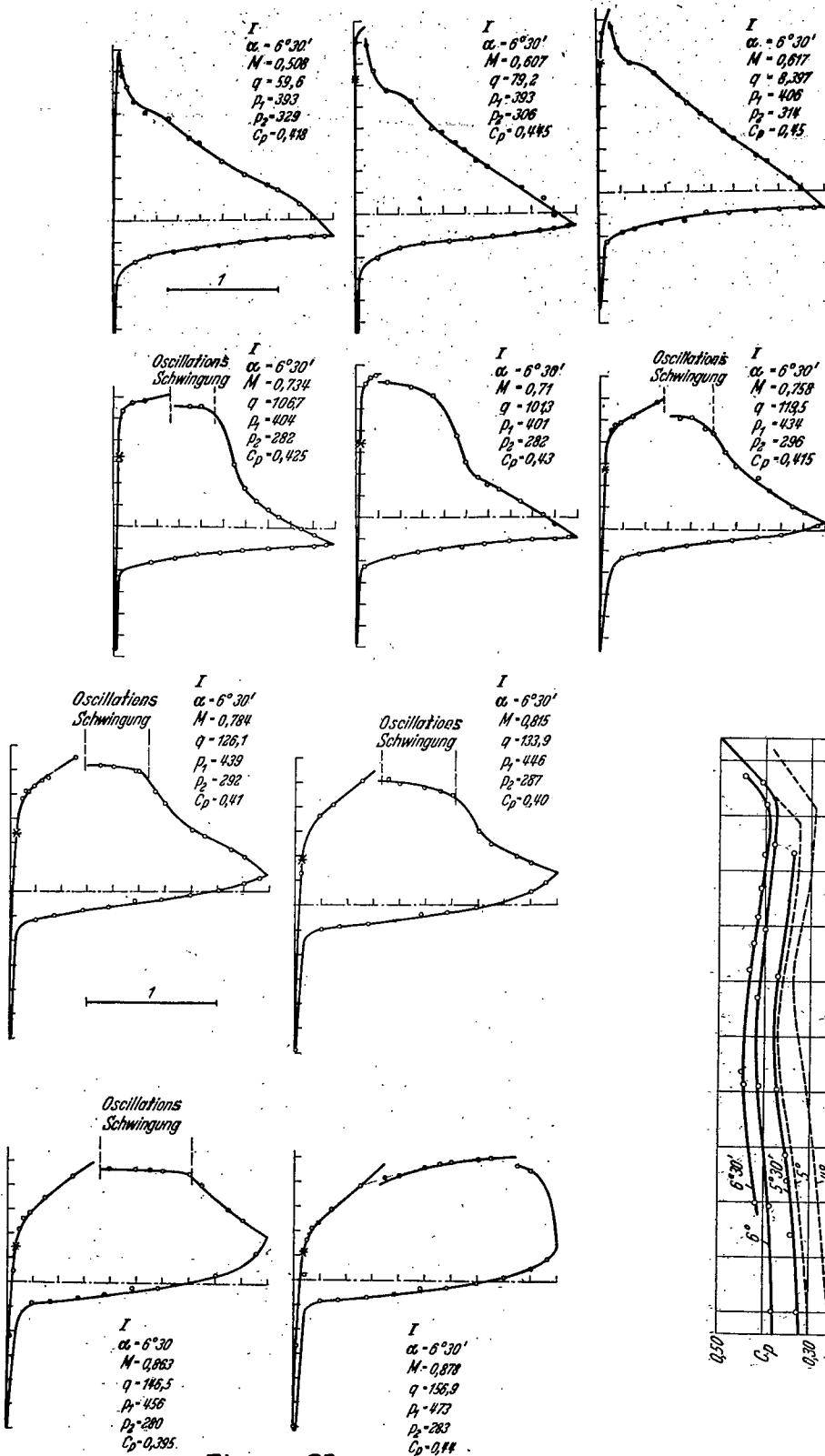


Figure 28.

Figure 29.

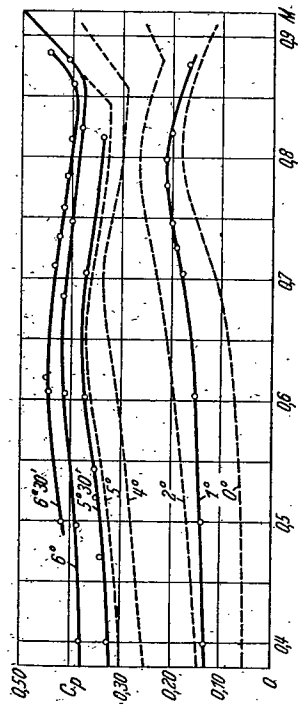


Figure 30.

LANGLEY RESEARCH CENTER



3 1176 00506 7070